A&A 430, 967–977 (2005)
DOI: 10.1051/0004-6361:20041589

Astronomy & Astrophysics

Deuterated molecular hydrogen in the Galactic ISM

New observations along seven translucent sightlines

S. Lacour[1,2,3], M. K. André[1], P. Sonnentrucker[2], F. Le Petit[4,5], D. E. Welty[6], J.-M. Desert[1], R. Ferlet[1], E. Roueff[5], and D. G. York[6]

[1] Institut d'Astrophysique de Paris, CNRS/UPMC, 98bis boulevard Arago, 75014 Paris, France
e-mail: sylvestre.lacour@obspm.fr
[2] Department of Physics and Astronomy, Johns Hopkins University, 3400 North Charles Street, Baltimore, MD 21218, USA
[3] Observatoire de Paris-Meudon, LESIA, 5 place Jules Janssen, 92195 Meudon, France
[4] Onsala Space Observatory, 43992 Onsala, Sweden
[5] Observatoire de Paris-Meudon, LUTH, 5 place Jules Janssen, 92195 Meudon, France
[6] Department of Astronomy and Astrophysics, University of Chicago, 5640 South Ellis Avenue, Chicago, IL 60637, USA

Received 2 July 2004 / Accepted 4 October 2004

Abstract. We present column density measurements of the HD molecule in the interstellar gas toward 17 Galactic stars. The values for the seven most heavily reddened sightlines, with $E(B-V) = 0.38-0.72$, are derived from observations with the *Far Ultraviolet Spectroscopic Explorer* (*FUSE*). The other ten values are from a reanalysis of spectra obtained with *Copernicus*. In all cases, high-resolution ground-based observations of K I and/or the CH molecule were used to constrain the gas velocity structure and to correct for saturation effects. Comparisons of the column densities HD, CH, CN, and K I in these 17 sightlines indicate that HD is most tightly correlated with CH. Stringent lower limits to the interstellar D/H ratio, derived from the HD/2H_2 ratio, range from 3.7×10^{-7} to 4.3×10^{-6}. Our results also suggest that the HD/H_2 ratio increases with the molecular fraction $f(H_2)$ and that the interstellar D/H ratio might be obtained from HD by probing clouds with $f(H_2) \sim 1$. Finally, we note an apparent relationship between the molecular fractions of hydrogen and deuterium.

Key words. ISM: abundances – ISM: clouds – ISM: lines and bands – ISM: molecules – ultraviolet: ISM

1. Introduction

It is believed that deuterium was produced in significant amounts only during the primordial Big Bang Nucleosynthesis. Since then, deuterium has been steadily destroyed in stellar interiors. Thus, its abundance relative to H, noted D/H, is a key measurement for studies of both cosmology and Galactic chemical evolution (Vangioni-Flam et al. 2000; Coc et al. 2004). D/H in the Interstellar Medium (ISM) is characteristic of the present-day Galactic deuterium abundance. Prior to the *FUSE* mission, $(D/H)_{ISM}$ showed some dispersion (e.g. Lemoine et al. 1999, for a review), likely resulting from poorly understood physical processes like astration, inefficient mixing, depletion onto grains, and perhaps some unidentified systematic errors. The final resolution of these issues will have strong implications for our understanding of the physics of the ISM, the chemical evolution of the Galaxy, and the baryonic density of the Universe inferred from primordial D/H.

An accurate determination of $(D/H)_{ISM}$ is one of the main goals of the *FUSE* mission. So far, most of these measurements have been performed within the Local Interstellar Medium (LISM). Moos et al. (2002) reviewed those and reported $(D/H)_{LB} = (1.52 \pm 0.08) \times 10^{-5}$ within the Local Bubble (LB). However, this value may not be representative of the true Galactic $(D/H)_{ISM}$. Hébrard & Moos (2003) used a D/O survey to constrain the D/H variations and, assuming a constant O/H ratio, obtained a D/H ratio below 1.0×10^{-5} outside the LB. Indeed, recent measurements suggest a "canonical" $(D/H)_{ISM}$, if it exists, likely 2 to 3 times lower (Jenkins et al. 1999; Sonneborn et al. 2000; Hoopes et al. 2003). Unfortunately, extended direct investigations over long Galactic disk sight lines are difficult, due to saturation and blends with neighboring H I Lyman lines.

The HD/H_2 ratio is an interesting alternative for D/H investigations along long sightlines. In the diffuse ISM, the formation of HD occurs via the ion-neutral reaction:

$$H_2 + D^+ \longrightarrow HD + H^+$$

while its destruction is due to photodissociation. Because of the lower abundance of deuterium compared to hydrogen, self-shielding of HD becomes significant only at higher extinction

Table 1. Target list.

Star	α (J 2000)	δ (J 2000)	V (mag)	$E_{(B-V)}$[a]	Distance (pc)	Ref.	A_V (mag)[a]	Type
HD 27778	04 23 59.79	+24 18 03.6	6.33	0.38	220	1	1.01	B3V
HD 73882	08 39 09.53	−40 25 09.3	7.27	0.72	925	2	2.28	O9III
HD 110432	12 42 50.27	−63 03 31.0	5.32	0.40	430	3	1.32	B2IVpe
HD 185418	19 38 27.48	+17 15 26.1	7.52	0.51	790	4	2.03	B0.5V
HD 192639	20 14 30.43	+37 21 13.8	7.11	0.66	1800	5	1.87	O8e
HD 206267	21 38 57.62	+57 29 20.5	5.62	0.52	615	6	1.37	O6e
HD 207538	21 47 39.79	+59 42 01.3	7.30	0.64	615	6	1.43	B0V

References. – 1 = Simbad; 2 = Ferlet et al. (2000); 3 = van Dishoeck & Black (1989); 4 = Sonnentrucker et al. (2003); 5 = St.-Louis & Smith (1991); 6 = de Zeeuw et al. (1999).
[a] Reddening and visible extinction parameters from Rachford et al. (2002).

than for H_2. Therefore, the transition between atomic deuterium and HD takes place deeper in a cloud than the transition between atomic and molecular hydrogen. Whenever all the deuterium is in molecular form, the ratio $N(\mathrm{HD})/2N(\mathrm{H_2})$ should be equal to the elemental abundance ratio D/H (see also Watson 1973). Less than a dozen observations of deuterated molecular hydrogen have been carried out to date, from the first FUV detections with *Copernicus* thirty years ago (Spitzer et al. 1973; Black & Dalgarno 1973; Watson 1973) to infrared observations with *ISO* (Wright et al. 1999; Bertoldi et al. 1999). Recently, the higher sensitivity of the *FUSE* satellite has allowed detection of HD in extra-galactic sources (Bluhm & de Boer 2001; André et al. 2004). In addition, more heavily reddened clouds which previously could not be investigated in the FUV are now within reach, as shown by Ferlet et al. (2000) toward HD 73882 ($A_\mathrm{V} \approx 2.3$ mag).

In this work, we make use of FUV data obtained with *FUSE* towards seven early-type Galactic stars (see Table 1). Each sightline is "translucent", i.e., showing significant extinction (1 mag $< A_\mathrm{V} <$ 5 mag; see Rachford et al. 2002). Because of the high sensitivity of *FUSE* (10 000 times more sensitive than *Copernicus*; Moos et al. 2000), the data have good S/N ratios, which allow accurate measurements of equivalent widths. However, at the large column densities needed to have most of the deuterium in molecular form, most of the HD lines available will be strongly saturated. Prior knowledge of the sightline velocity structure is therefore crucial for the analysis. We made use of available very high resolution optical data for CH – known to be a good tracer of H_2 (Danks et al. 1984; Magnani et al. 1998) – in order to constrain the gas velocity structure toward our target stars.

In the next section we describe the criteria used to select the targets and note some interesting aspects of each of the seven lines of sight. In Sects. 3 and 4, we present the FUV observational data and our methods of reduction and analysis. In Sect. 5, we discuss the inferred deuterium abundances.

2. The sample

The target selection was based on three criteria: a significant extinction ($A_\mathrm{V} > 1$ mag), the availability of high resolution data for the CH molecule, and a good S/N ratio ($\gtrsim$10 per pixel) in the *FUSE* data. The targets of the *FUSE* P116 program ("Survey of H_2 in Translucent Clouds"; Snow et al.) fulfilled the first two criteria. We retained for this survey the seven sightlines with the best S/N (listed in Table 1).

HD 27778 is located behind the outer portion of L1506 (Lynds 1962). The chemistry of this region was investigated by Federman et al. (1994). Their model suggests a low UV flux (which is likely a consequence of the filamentary structure of the ISM in Taurus region), as well as an average density inside the cloud of nearly 900 cm^{-3}.

HD 73882 is very interesting for translucent cloud studies since it is a very bright early type star that allows us to probe dense material with high S/N. It is believed that this sightline is dominated by one or more dense clouds consistent with translucent cloud models (Snow et al. 2000).

HD 110432 lies beyond the Coalsack dark nebula. Its average reddening ($A_\mathrm{V} = 1.32$ mag, see Rachford et al. 2001) makes it intermediate between diffuse and translucent lines of sight.

HD 185418 is a B0.5V star at 790 pc from the Sun (Fitzpatrick & Massa 1988, 1990). While its high reddening suggested the potential existence of translucent clouds along the sightline, a recent detailed study of the gas physical conditions showed that the sightline is instead comprised of multiple diffuse components (Sonnentrucker et al. 2003).

HD 192639 is a member of the Cyg OB1 association. As for HD 185418, the study of the physical conditions along the sightline has revealed it to be dominated by an ensemble of diffuse clouds (Sonnentrucker et al. 2002).

HD 206267 is a quadruple system within the Cepheus OB association cluster Trumpler 37. Both the cluster and the associated H II region IC1396 have been well studied (Morbidelli et al. 1997). It is believed that most of the intervening material is foreground, with a small contribution from IC1396. Spectra of three of the stars in the system (Pan et al. 2001) reveal substantial variations for CN on sub-parsec scales, but smaller variations for CH (less than 20%).

HD 207538 also is in the Cepheus OB2 association (Humphreys 1978). Polarization data show that this line of sight has a small R_V, but otherwise very little is known about its ISM content (Catanzaro et al. 2003).

Table 2. Log of *FUSE* observations.

Star	*FUSE* ID [a]	Start Date	Number of exposures	Exposure time (ks)	S/N [b] (λ 1070 Å)
HD 27778	P1160301	2000.10.27	4	9.7	10.8
HD 73882	P1161301	2000.01.24	6	11.9	5.1
···	P1161302	2000.03.19	8	13.6	4.6
HD 110432	P1161401	2000.04.04	5	3.6	28.5
HD 185418	P1162301	2000.08.10	3	4.4	14.9
HD 192639	P1162401	2000.06.12	2	4.8	8.1
HD 206267	P1162701	2000.07.21	3	4.9	10.2
HD 207538	P1162902	1999.12.08	4	7.7	6.2
···	P1162903	2000.07.21	10	11.2	7.1

[a] Archival root name of targets from *FUSE* PI team observations.
[b] Average per-pixel S/N for a 1 Å region of the LIF 1A spectrum near λ 1070 Å.

3. Observations and data analysis

3.1. FUSE data

The *FUSE* mission, its planning, and its on-orbit performance are discussed by Moos et al. (2000) and Sahnow et al. (2000).

The list of the 7 targets studied in this work and the observation information are given in Tables 1 and 2, respectively. All data were obtained with the source centered in the $30'' \times 30''$ (LWRS) aperture, with total exposure times ranging from 3.6 ks (HD 110432) to 25.5 ks (HD 73882). All our datasets have a S/N ratio per pixel between 10 and 30. All the data were processed with version 2.0.4 of the CalFUSE pipeline[1]. Correction for detector background, Doppler shift, geometrical distortion, astigmatism, dead pixels, and walk were applied. No correction was made for the fixed-pattern noise. The 1D spectra were extracted from the 2D spectra using optimal extraction (Horne 1986; Robertson 1986). The 1D spectra from individual exposures were cross-correlated and co-added for each detector segment. Equivalent width measurements were performed independently for the spectra from each segment. Since the nominal spectral resolution is $\approx$20 km s^{-1} (*FWHM*), we binned the data by 4 pixels ($\approx$7 km s^{-1}) to increase the S/N ratio. All processed data have therefore a S/N per element greater than 20.

3.2. Ground based observations

For HD 73882 and HD 110432, high resolution CH spectra were obtained with the 3.6 m telescope at ESO, La Silla, using the CES spectrograph during one run in 2001 February. The reduction of the data was done using a homemade IDL package. First, we subtracted a mean bias value from each spectrum, then made adjustments to account for the background radiation. After flatfielding by means of spectra from a quartz flatfield lamp to remove the pixel-to-pixel sensitivity variations inherent to the detector, we used spectra from a Th–Ar hollow cathode lamp to determine the wavelength calibration. The resolution was estimated at 3 km s^{-1} from the widths of the thorium lines in the Th–Ar exposures.

For the other stars, high-resolution (*FWHM* $\sim$ 1.2–2.0 km s^{-1}) spectra of K I, Na I, Ca I, Ca II, CN, CH, and CH^+ were obtained with the Kitt Peak coudé feed telescope in various runs from 1995 to 2000. A detailed discussion of the reduction and analyses of these spectra – and of similar spectra for other stars in the *FUSE* translucent cloud survey (Rachford et al. 2002) – will be given by Welty et al. (in preparation).

[1] http://fuse.pha.jhu.edu/analysis/analysis.html

4. Column density measurements

Due to its dipole moment, HD is primarily detected through transitions from the ground rotational state $J = 0$. There are 20 Lyman and 6 Werner $HD_{J=0}$ transitions in the *FUSE* wavelength range (Dabrowski & Herzberg 1976). In Fig. 1, we plot the spectrum of HD 110432 from 1000 Å to 1110 Å. Many absorption lines are detected, most of them due to molecular hydrogen. The upper tick marks indicate the H_2 $J = 1$ to 4 lines and the thick tick marks indicate the HD $J = 0$ Lyman lines. Most of the HD transitions cannot be detected because either they are too close to the saturated H_2 ($J = 0$ and $J = 1$) absorption lines or they are blended with atomic lines. Therefore, only 7 HD transitions between 959 Å and 1106 Å could be used (see Table 3). The wavenumbers have been determined through absorption and emission spectroscopy by Dabrowski & Herzberg (1976). Abgrall & Roueff (2004, to be submitted) have calculated the transition energies, the oscillator strengths, and total radiative lifetimes in the Lyman and Werner band systems by following a similar approach to the one used for H_2 (Abgrall et al. 1993a,b, 2000). The rest wavelengths and oscillator strengths for the HD lines seen toward the seven sightlines studied here are listed in Table 3. Experimental wavelengths have been used when available; the typical accuracy on the transition wavenumbers is within one wavenumber.

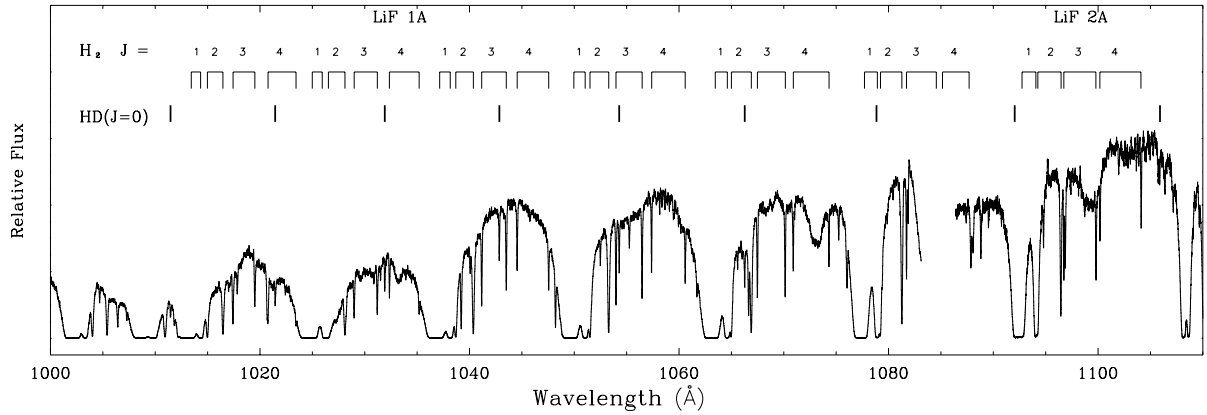

Fig. 1. *FUSE* spectrum of HD 110432 from 1000 to 1110 Å. Many molecular absorption lines are detected, most of them belonging to molecular hydrogen. The upper tick marks indicate the position of H_2 lines from $J = 1$ to 4. The thick tick marks indicate the position of the HD $J = 0$ Lyman lines. H_2 lines from the ground and the first rotational states are strongly saturated, consistent with the high reddening in this line of sight. The gap around 1085 Å is due to the gap between the two microchannel plates mounted in the LiF 1A and LiF 2A detectors.

Table 3. Equivalent widths of HD lines used in this work.

Star	$W(959)$ (mÅ)	$W(975)$ (mÅ)	$W(1011)$ (mÅ)	$W(1021)$ (mÅ)	$W(1054)$ (mÅ)	$W(1066)$ (mÅ)	$W(1105)^a$ (mÅ)
HD 27778	27 ± 11		34 ± 6	34 ± 8	38 ± 4	42 ± 4	15 ± 6
HD 73882				43 ± 9	45 ± 4	44 ± 5	16 ± 4
HD 110432	29 ± 3		34 ± 3	32 ± 2	34 ± 3	34 ± 3	12 ± 3
HD 185418	31 ± 5		58 ± 6	62 ± 16	48 ± 6	53 ± 6	21 ± 5
HD 192639	48 ± 7	42 ± 5	49 ± 4	52 ± 3	53 ± 3		15 ± 7
HD 206267	47 ± 4	43 ± 4	49 ± 4	53 ± 3	55 ± 3	47 ± 3	20 ± 8
HD 207538	38 ± 6			45 ± 4	49 ± 3	55 ± 4	27 ± 9
Line	L14-0R(0)	L12-0R(0)	L8-0R(0)	L7-0R(0)	L4-0R(0)	L3-0R(0)	L0-0R(0)
λ_0	959.82	975.58	1011.46	1021.46	1054.29	1066.27	1105.86
f	0.0147	0.0196	0.0262	0.0254	0.0164	0.0115	0.000744

[a] Slight blend with C I* has been accounted for.

Two methods were used to obtain HD column densities: the curve of growth method (hereafter COG) and the profile fitting method (hereafter PF).

4.1. Curve of growth method

The equivalent widths (EqW) of the HD lines studied in this work are summarized in Table 3. The stellar continuum in the vicinity of each line was estimated using a low-order Legendre polynomial to fit the data. The error bars given here are 1σ (see Sect. 4.3).

Most of the lines have similar oscillator strengths and show a large degree of saturation. It is therefore crucial to have accurate information on the velocity structure of the gas for these lines of sight. Because the integrated sightline column densities of CH and H_2 are generally very well correlated (Danks et al. 1984; van Dishoeck & Black 1989; Magnani et al. 1998), we used the CH structure to generate multi-component curves of growth for HD. Because K I is generally well correlated with both CH and H_2 and also (being heavier) exhibits smaller thermal broadening, it can be used to discern even more complex structure (Welty & Hobbs 2001). Toward HD 73882, for example, we used the five-component structure found for K I to fit both CH and HD.

The multi-component curves of growth are obtained by integrating multiple Voigt profiles, each of which corresponds to one gas component. Each component is defined by a b-value, a radial velocity, and a column density. For each component, the radial velocity is taken equal to that of the CH, and the column density is proportional to that of CH. Because HD and CH differ in mass (3 vs. 13 amu), we modified b as follows:

$$b_{\rm HD} = \sqrt{b_{\rm CH}^2 + 2kT\left(\frac{1}{m_{\rm HD}} - \frac{1}{m_{\rm CH}}\right)}. \quad (1)$$

The temperature of the gas is calculated from the two lower rotational states of H_2 (Rachford et al. 2002). Table 4 lists the adopted component structures and the H_2 gas temperature T_{01}.

Figure 2 shows the best COG fit to the measured equivalent widths. The weak line at 1105.86 Å is important. Its very low oscillator strength (almost one hundred times smaller than the others) makes it nearly optically thin. However, blending with

Table 4. Assumed component structure.

Star	T_{01}[a] (K)	Model	Component	Relative strength	$v_{\rm HEL}$ km s^{-1}	$b_{\rm CH}$ km s^{-1}	$b_{\rm HD}$[b] km s^{-1}
HD 27778	55	CH	1	0.47	14.6	1.1	1.3
			2	0.53	17.1	2.0	2.1
HD 73882	51	K I/CH	1	0.25	20.5	0.9	1.1
			2	0.45	22.1	0.9	1.1
			3	0.24	23.7	0.9	1.1
			4	0.04	25.5	1.1	1.3
			5	0.02	28.7	1.0	1.2
HD 110432	68	CH[c]	1	0.32	2.9	1.7	1.8
			2	0.67	6.9	1.3	1.5
HD 185418	101	CH	1	0.59	−10.40	1.3	1.5
			2	0.41	−6.20	2.5	2.7
HD 192639	98	CH	1	0.56	−16.0	3.7	3.8
			2	0.44	−10.0	2.1	2.3
HD 206267	65	CH	1	0.50	−17.5	2.6	2.7
			2	0.30	−13.2	1.0	1.2
			3	0.20	−10.1	2.1	2.2
HD 207538	73	CH	1	0.19	−19.3	0.8	1.1
			2	0.35	−16.6	0.8	1.1
			3	0.38	−13.5	1.2	1.4
			4	0.08	−10.2	1.2	1.4

[a] T_{01} are from the *FUSE* H_2 Survey (Rachford et al. 2002). [b] See Sect. 4.1. [c] Crawford (1995).

a line due to C I* hindered accurate measurement of its equivalent width, as reflected by the larger error bars. Nevertheless, because this is the only line not significantly saturated, we doubled its weight in the COG fits to increase its impact compared to that of the saturated lines.

4.2. Profile fitting method

We also used a profile fitting program called *Owens* (Lemoine et al. 2002; Hébrard et al. 2002), developed by M. Lemoine at the Institut d'Astrophysique de Paris, to estimate the HD column densities. This program allows us both to fit all the HD lines simultaneously (performing a global χ^2 minimization) and also to add other species (e.g., C I* and C II** to deblend the 1105.86 Å line). Because of the significant saturation of the other HD lines, we used the velocity distribution of the CH components to constrain our fit, as for the COG. But unlike the COG technique, profile fitting (PF) allows us to leave both the *b*-value and relative strength as free parameters for each component. This approach is more realistic, because even though HD appears to be correlated with CH (see below), the correlation is not perfect. The best fits for several absorption lines toward HD 110432 are shown in Fig. 3. These fits indicate clearly the importance of adding the C I* 1105.73 Å line to deblend the HD 1105.86 Å line; the profile fitting technique allows us to better disentangle the absorption from the two species. The derived 1σ error bars are discussed in the following section.

4.3. Error estimation

We considered four basic types of errors, which are calculated differently depending on the method used:

The statistical errors are assumed to be a Poissonian noise. Those errors (roughly the square root of the count rate) are computed by the CalFUSE pipeline for each pixel. For the COG technique, we obtained the total statistical error by summing in quadrature the error for each integrated pixel (more information can be found in Appendix A of Sembach & Savage 1992). For the PF technique, this error is used by *Owens* to calculate the χ^2.

The background uncertainties are proportional to exposure time. The *FUSE* science data processing team assumed it to be close to 10% of the computed background[2]. This error is calculated by the pipeline and added to the statistical errors.

When using the PF technique, *Owens* optimizes the continua over all the HD lines at once, so that **the continuum placement error** is included automatically in the χ^2. The measurement of EqWs, however, requires a prior determination of the continuum, and in that case, the continuum error depends mainly upon the S/N ratio in the vicinity of the line. To estimate it, we shifted the continuum by 1 to 3% (depending on the S/N ratio; see Sembach & Savage 1992), and determined lower and upper values for the EqW. The maximum difference is considered as our 1σ error.

[2] http://fuse.pha.jhu.edu/analysis/calfuse_wp3.html

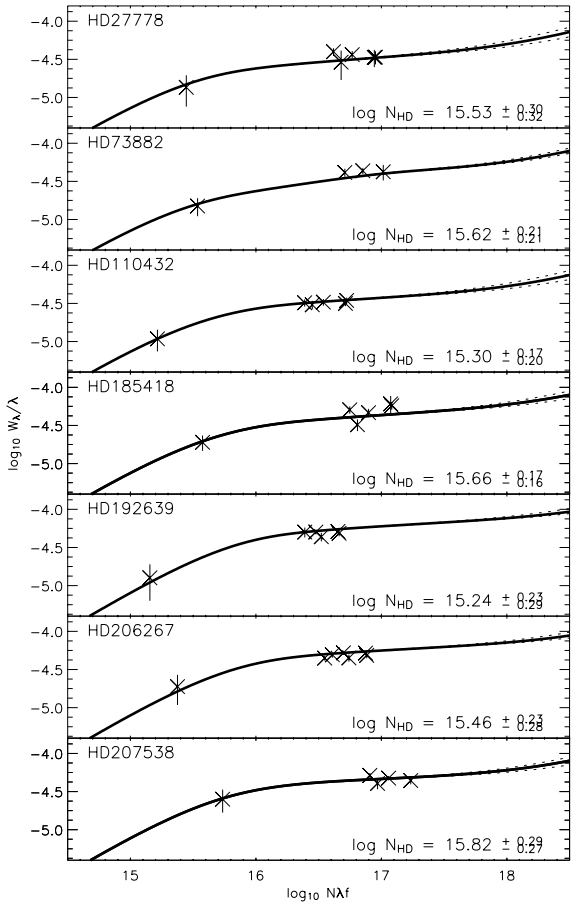

Fig. 2. Curves of growth for each of the seven lines of sight. The strong saturation of all but one of the HD lines indicates that it is necessary to use accurate information on the velocity structure of the gas to derive N(HD) for our lines of sight. We fitted our equivalent widths (EqWs) on the curves of growth obtained from the CH structure (see Sect. 4.1). The unsaturated HD line at 1105.86 Å has a large error bar because of blends.

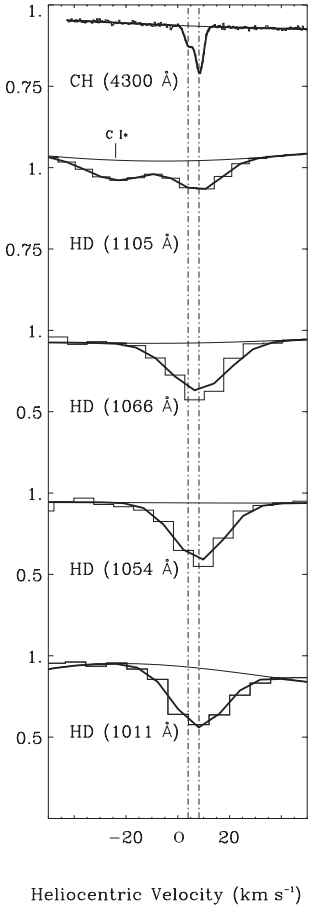

Fig. 3. This figure shows the 2-component profile fitting of the HD lines toward HD 110432. Plotted are the HD lines present in the *FUSE* LiF 1A and LiF 1B channels as well as the fit of the CH absorption lines from the CES data (at 3 km s^{-1}). Although clearly seen in the CES data, the velocity shift of 4 km s^{-1} between the two CH components would have remained undetected using the *FUSE* data alone.

Table 5. *FUSE* HD column densities.

Star	N(HD)[a]		
	FIT	COG	Mean
HD 27778	$3.0^{+2.9}_{-1.7}$	$3.4^{+3.4}_{-1.8}$	$3.2^{+3.2}_{-1.7}$
HD 73882	$7.4^{+4.9}_{-5.2}$	$4.2^{+2.6}_{-1.6}$	$5.8^{+3.7}_{-3.4}$
HD 110432	$1.9^{+0.5}_{-0.4}$	$2.0^{+1.0}_{-0.7}$	$1.9^{+0.7}_{-0.6}$
HD 185418	$4.0^{+1.5}_{-0.8}$	$4.6^{+2.2}_{-1.4}$	$4.3^{+1.9}_{-1.1}$
HD 192639	$1.2^{+0.6}_{-0.5}$	$1.7^{+1.2}_{-0.8}$	$1.5^{+0.9}_{-0.7}$
HD 206267	$1.3^{+1.0}_{-0.6}$	$2.9^{+2.0}_{-1.4}$	$2.1^{+1.5}_{-1.0}$
HD 207538	$3.5^{+3.9}_{-1.8}$	$6.6^{+6.3}_{-3.1}$	$5.0^{+5.1}_{-2.4}$

[a] All column densities are times 10^{15}.

The systematic errors are the most difficult errors to quantify. They may come from geometrical distortion, walk, dead pixels, point spread function (PSF) or fixed pattern noise. While most of these are corrected by the pipeline, small residual effects may influence our measurements. Moreover, there is no way to judge their influence over a single absorption line. To estimate these possible systematic errors, we have assumed that (1) they are proportional to the quadratic sum of the previously calculated errors; and (2) the number of measurements performed by each method is statistically significant (i.e., they have a reduced χ^2 equal to 1). Under those assumptions, we account for systematic errors by scaling the previous error to have the minimum χ^2 equal to the degrees of freedom. The χ^2 used for calculating the error with the PF method is implicit. For the COG technique, the χ^2 is obtained by fitting our points on the multi-component curve of growth.

There is an additional uncertainty which has the potential to exceed the ones already accounted for. It has to do with the goodness of the tracer that we used to model the HD lines. Because of the high *S/N* of our optical data, the CH component structures seem fairly well determined. However, it is likely that the HD components do not match perfectly those of CH. Because the degree of such differences is unknown, the resulting uncertainty could not be included in the stated error bars. We note, however, that the current determination of the HD column density allows a confirmation a posteriori of the quality of our tracer.

Table 6. *Copernicus* HD equivalent widths and column densities.

Star	N(HD) [a]	Inferred EqWs [a]		Literature EqWs		N(HD)	Ref.	New EqWs		New N(HD)	ΔN(HD)
		1054	1066	1054	1066			1054	1066		(dex)
HD 21278	14.06	18.5								14.2(0.1)	+0.15
o Per					31.0(2.0)	15.77	1			15.5(0.3)	−0.25
ζ Per	14.30	32.2		41.4(4.9)		15.60	2	27.7(2.6)		15.6(0.2)	+1.30
ϵ Per	13.57	6.0						6.6(0.4)		13.8(0.1)	+0.25
ξ Per	14.15	22.8	16.4					22.9(0.6)	17.5(1.1)	14.4(0.1)	+0.25
α Cam	14.49	49.9	35.8					52.0(2.0)	48.4(2.3)	14.9(0.1)	+0.40
139 Tau	13.84	11.2						8.5(1.0)		13.9(0.1)	+0.05
ζ Oph	14.23	27.4	19.7	20.6(1.6)	15.9(0.8)	14.26	3	18.8(1.0)	14.6(0.6)	14.8(0.3)	+0.55
59 Cyg	13.86	11.7						8.8(1.1)		13.9(0.1)	+0.05
10 Lac	14.41	41.5	29.7					5.5(0.7)	[3.3(1.0)]	13.5(0.2)	−0.90

References. – 1 = Snow (1975, 1976); 2 = Snow (1977); 3 = Wright & Morton (1979).
Note. – Errors on new equivalent widths (EqW) are 1-sigma.
[a] Spitzer et al. (1973); equivalent widths inferred from listed N(HD) and f-values of Allison & Dalgarno (1969), assuming optically thin lines (see Sect. 5.1).

5. Results and discussion

The values of N(HD) obtained for the 7 *FUSE* lines of sight are summarized in Table 5. There is good agreement between the column densities determined using both the COG and the PF techniques. In these particular cases, similar values are obtained by fixing only the component velocity distribution (PF) and by fixing in addition the relative strengths and the broadening of the CH components (COG). This agreement gives an indication of the reliability of our results. For the discussion below, we adopt the unweighted mean of the column densities determined by the two techniques.

5.1. Relation between CH and HD

The good correlation found between the column densities of CH and H_2 in diffuse interstellar clouds is consistent with the production of most of the CH via a network of gas phase reactions in which H_2 is a major component (Danks et al. 1984). This correlation recently was extended to more heavily reddened sightlines observed with *FUSE* (Rachford et al. 2002). The relatively tight relationship between these two species and the inferred chemical link both suggest that CH can be used as a tracer of H_2. Because HD is also produced through gas phase reactions with H_2 and because both CH and HD are subject to destruction through photoprocesses, one could assume that CH would be a good tracer for HD as well. To test this assumption, we plotted the column densities of H_2 versus HD, and H_2 and HD versus CH; this for all the Galactic lines of sight having estimates for N(HD). The sample includes ten sightlines observed with *Copernicus* (Spitzer et al. 1973; Snow 1975, 1976, 1977; Wright & Morton 1979) (see below) and the seven *FUSE* sightlines analyzed in the present work.

Because the N(HD) originally given by Spitzer et al. (1973) were estimated assuming the HD lines (at 1054 and/or 1066 Å) to be optically thin, those values should be taken as lower limits to the true N(HD). We therefore have re-examined all the *Copernicus* data and have derived new estimates for N(HD), using a method similar to that used for analyzing the *FUSE* spectra. The *Copernicus* U1 scans encompassing the HD lines at 1054 and/or 1066 Å were obtained from the MAST archive. Background levels were estimated from scans of nearby saturated H_2 lines obtained in the same observing programs. The equivalent widths measured from the normalized spectra (Table 6) are generally in good agreement with those inferred from the N(HD) listed by Spitzer et al. (1973) and with the values listed by Wright & Morton (1979). The most notable exception to that agreement is 10 Lac, where we suspect that the absorption near the HD line at 1054 Å is due mostly to stellar Fe III and/or Cr III (Rogerson & Upson 1977; Rogerson & Ewell 1985); there is no strong absorption at the expected position of the HD line at 1066 Å. (Spitzer et al.'s value for N(HD) toward 10 Lac was surprisingly high, given the modest $E_{(B-V)}$ and molecular fraction.) Component structures derived from high-resolution spectra of CH, K I, and/or Na I were used to model the profiles and/or equivalent widths of the HD lines (λ1054, λ1066, and others as available).

Our "new" *Copernicus* N(HD) are listed in the last column of Table 6 and plotted with open squares in Fig. 4. In most cases, the new values are higher than those listed by Spitzer et al. (1973) by factors of order 2; the value for ζ Oph is about 4 times higher. On the other hand, the new value for 10 Lac is about a factor of 8 smaller, and the value for o Per is about a factor of 2 smaller than that given by Snow (1975, 1976). We note that these new values could still underestimate the true N(HD) if HD is actually concentrated in fewer components than the tracer used to model the HD equivalent widths.

Table 7 summarizes the correlations between several different species. As shown in Fig. 4, it suggests a good correlation between HD and H_2, and between H_2 and CH. Thus it is no surprise that it indicates a correlation between HD and CH column densities, but with a slope somewhat steeper

Table 7. Correlation plots.

Quantities	r [a]	N [b]	Slope [c]
HD vs. H_2	0.923	16	1.29 ± 0.14
H_2 vs. CH	0.911	12	1.18 ± 0.19
HD vs. CH	0.807	13	1.94 ± 0.44
HD vs. CN	0.732	9	0.66 ± 0.15
HD vs. K I	0.745	14	0.86 ± 0.20
$HD/2H_2$ vs. H_2	0.291	16	0.05 ± 0.13
f(HD) vs. $f(H_2)$ – $(D/H)_{ISM}$ = 0.74e−5	0.725	16	$0.40 \pm .10$
f(HD) vs. $f(H_2)$ – $(D/H)_{ISM}$ = 1.52e−5	0.725	16	$0.19 \pm .05$

[a] Linear correlation coefficient.
[b] Number of points (detections only).
[c] Slope and uncertainty of weighted least-squares linear fit, considering uncertainties in both quantities.

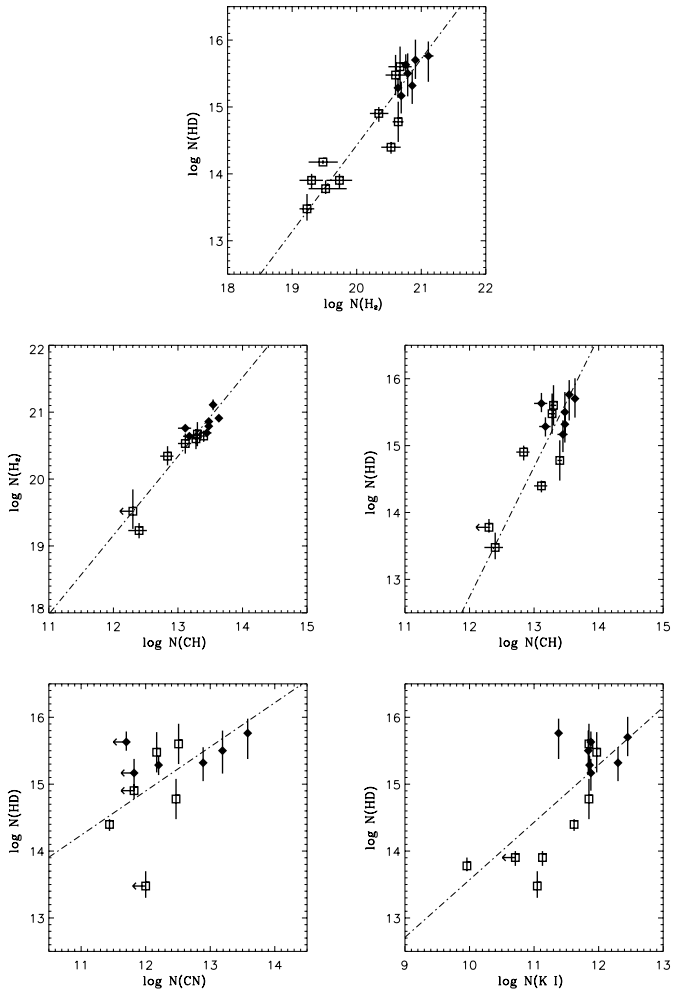

Fig. 4. (*Top*) N(HD) vs. $N(H_2)$: the correlation factor close to 1 comfirmes a good correlation between the two species, as predicted by chemical models (Danks et al. 1984). The slope is slightly greater than 1.0. – (*Middle*) $N(H_2)$ and N(HD) vs. N(CH): tight correlation between $N(H_2)$ and N(CH) was already observed in wide survey (Rachford et al. 2002), and appears in the left panel with a slope close to 1. N(HD) vs. N(CH) also shows a good relationship, but with a slope near 2.0. – (*Bottom*) N(HD) vs. N(CN) and N(K I): none of the species exhibit a tight relationship. – Filled diamonds have N(HD) derived from *FUSE* spectra; open squares have N(HD) derived from reanalysis of *Copernicus* data. All the correlation factors and slopes are summarized in Table 7.

than that for $N(H_2)$ vs. N(CH). There are few points with $N(\mathrm{HD}) \lesssim 10^{15}$ cm^{-2}, however, so it would be very useful to obtain more measurements of HD (and CH) at those lower column densities. We also investigated whether CN and K I might be useful as tracers for HD, as all three species are expected to be concentrated in the denser parts of diffuse clouds. In addition, K I is generally more readily detected than CH and typically reveals more details of the component structure (e.g., Welty & Hobbs 2001). Bottom panels of Fig. 4 show HD vs. CN and K I. While CN and K I show some degree of correlation with HD, the relationships are not as tight as that with CH.

5.2. The D/H ratio

Using the Meudon PDR model (Nehmé et al. to be published), Le Petit et al. (2002) studied the properties of HD in a diffuse cloud with $n_{\mathrm{H}} = 500$ cm^{-3} embedded in the standard interstellar radiation field. Under those conditions, HD becomes the reservoir of deuterium at a visual extinction of 1 mag, where the molecular fraction $f(H_2)$ of hydrogen is close to 1. Toward our sightlines, $f(H_2)$ does not reach such a value. However, if we assume in each case that (1) a significant part of the atomic hydrogen is not associated with the observed diffuse molecular material; and (2) all the molecular material is in one dominant cloud, then the D/H ratio in that main cloud should be equal to the $N(\mathrm{HD})/2N(H_2)$ ratio.

Table 8 shows the $N(\mathrm{HD})/2N(H_2)$ ratios for all the sightlines included in this paper, i.e., our *FUSE* measurements and the values we have re-derived from the *Copernicus* data. All these values are plotted in Fig. 5, where we have added two reference values: the Local Bubble $N(\mathrm{D})/N(\mathrm{H})$ ratio of 1.52×10^{-5} (Moos et al. 2002), and the Jenkins et al. (1999) value of 0.74×10^{-5} toward δ Ori A (First detection by Laurent et al. 1979). Several recent observations (Hébrard & Moos 2003; Hoopes et al. 2003; Wood et al. 2004) have suggested that the LB value may not be representative of the general ISM and that a "canonical" $(D/H)_{ISM}$ (if such exists) may be closer to the latter value. For our sample, the average $N(\mathrm{HD})/2N(H_2)$ yields a corresponding estimate for D/H of $(2.0\pm1.1)\times10^{-6}$, a factor 7 below the LB value and a factor 3 below the δ Ori A value. Such a low value is difficult to interpret in terms of enhanced stellar astration or favored deuterium depletion onto dust grains. Indeed, given the multi-component velocity structure of the sightlines and the many special conditions that may change the HD/H_2 ratio from component to component, the most likely explanation is that we have not yet identified a predominantly molecular cloud.

We now turn to a more realistic view of the sightlines in which several molecule-containing clouds are present, with only some of them having all the deuterium in the molecular form. To some extent we can expect that the molecular

Table 8. Column densities.

Star	$E_{(B-V)}$	$f(H_2)$ [a]	$N(H\,I)$ [cm^{-2}]	$N(H_2)$ [cm^{-2}]	$N(HD)$ [cm^{-2}]	Ref.	$N(HD)/2N(H_2)$	$N(CH)$ [cm^{-2}]	Ref.
HD 27778	0.38	0.57	$9.5^{+9.5}_{-4.8}$ (20)	$6.2^{+0.9}_{-0.8}$ (20)	$3.2^{+3.2}_{-1.7}$ (15)	1	$2.6^{+2.6}_{-1.4}$ (-6)	3.0 ± 0.3 (13)	2
HD 73882	0.72	0.67	$1.3^{+0.5}_{-0.4}$ (21)	$1.3^{+0.3}_{-0.2}$ (21)	$5.8^{+3.7}_{-3.4}$ (15)	1	$2.2^{+1.6}_{-1.3}$ (-6)	3.5 ± 0.4 (13)	2
HD 110432	0.40	0.55	$7.1^{+2.9}_{-2.1}$ (20)	$4.4^{+0.4}_{-0.4}$ (20)	$1.9^{+0.7}_{-0.6}$ (15)	1	$2.2^{+0.9}_{-0.7}$ (-6)	1.5 ± 0.3 (13)	3
HD 185418	0.51	0.47	$1.3^{+0.5}_{-0.4}$ (21)	$5.8^{+0.7}_{-0.6}$ (20)	$4.3^{+1.9}_{-1.1}$ (15)	1	$3.7^{+1.7}_{-1.0}$ (-6)	1.3 ± 0.3 (13)	2
HD 192639	0.66	0.32	$2.1^{+0.7}_{-0.5}$ (21)	$4.9^{+0.6}_{-0.5}$ (20)	$1.5^{+0.9}_{-0.7}$ (15)	1	$1.5^{+1.0}_{-0.7}$ (-6)	2.8 ± 0.5 (13)	2
HD 206267	0.52	0.42	$2.0^{+0.8}_{-0.6}$ (21)	$7.2^{+0.7}_{-0.6}$ (20)	$2.1^{+1.5}_{-1.0}$ (15)	1	$1.4^{+1.0}_{-0.7}$ (-6)	3.0 ± 0.2 (13)	2
HD 207538	0.64	0.42	$2.2^{+0.7}_{-0.5}$ (21)	$8.1^{+0.8}_{-0.7}$ (20)	$5.0^{+5.1}_{-2.4}$ (15)	1	$3.1^{+3.2}_{-1.5}$ (-6)	4.3 ± 0.2 (13)	2
HD 21278	0.10	0.10 [b]	5.5 (20) [b]	$3.0^{+2.1}_{-1.2}$ (19)	$1.5^{+0.1}_{-0.1}$ (14)	4	$2.5^{+1.7}_{-1.0}$ (-6)		
o Per	0.30	0.50	8.0 ± 2.4 (20)	$4.0^{+1.6}_{-1.2}$ (20)	$3.0^{+3.0}_{-1.5}$ (15)	4	$3.8^{+4.4}_{-2.0}$ (-6)	2.1 ± 0.2 (13)	5
ζ Per	0.33	0.59	6.4 ± 0.6 (20)	$4.7^{+2.4}_{-1.6}$ (20)	4^{+4}_{-2} (15)	4	$4.3^{+5.3}_{-2.4}$ (-6)	2.2 ± 0.2 (13)	5
ϵ Per	0.09	0.21	2.5 ± 0.5 (20)	$3.3^{+2.7}_{-1.5}$ (19)	6^{+2}_{-1} (13)	4	$9.1^{+8.7}_{-4.9}$ (-7)	< 2.0 (12)	6
ξ Per	0.33	0.35	1.3 ± 0.3 (21)	$3.4^{+1.4}_{-1.0}$ (20)	$2.5^{+0.5}_{-0.5}$ (14)	4	$3.7^{+1.8}_{-1.2}$ (-7)	1.3 ± 0.3 (13)	5
α Cam	0.32	0.35	8.0 ± 1.6 (20)	$2.2^{+0.9}_{-0.6}$ (20)	8^{+2}_{-2} (14)	4	$1.8^{+0.9}_{-0.7}$ (-6)	6.9 ± 1.6 (12)	5
139 Tau	0.15	0.12	8.0 ± 1.6 (20)	$5.4^{+3.1}_{-2.0}$ (19)	8^{+2}_{-2} (13)	4	$7.4^{+5.0}_{-3.1}$ (-7)		
ζ Oph	0.32	0.63	5.2 ± 0.3 (20)	$4.4^{+0.9}_{-0.8}$ (20)	6^{+6}_{-3} (14)	4	$6.8^{+7.2}_{-3.5}$ (-7)	2.5 ± 0.2 (13)	5
59 Cyg	0.18	0.19	1.8 ± 0.4 (20)	$2.0^{+1.0}_{-0.7}$ (19)	8^{+2}_{-2} (13)	4	$2.0^{+1.2}_{-0.8}$ (-6)		
10 Lac	0.11	0.06	5.0 ± 1.5 (20)	$1.7^{+0.5}_{-0.4}$ (19)	3^{+2}_{-1} (13)	4	$8.8^{+6.9}_{-3.4}$ (-7)	2.5 ± 0.8 (12)	7

References. –1 = this paper (*FUSE* data); 2 = Welty et al., in prep.; 3 = Crawford (1995); 4 = this paper (*Copernicus* data); 5 = Thorburn et al. (2003), 6 = Federman et al. (1994); 7 = Thorburn, priv. comm.
Note. – (*nn*) stands for 10^{nn}.
[a] $f(H_2) = 2N(H_2)/(2N(H_2) + N(H\,I))$. – [b] Inferred from $E(B-V)$.

fraction $f(H_2)$ will be a relevant parameter. $f(H_2)$ will increase with the average UV shielding and decrease with the fraction of smaller, more diffuse molecular clouds present. The models suggest that the deuterium is molecular only when hydrogen is fully in its molecular form (Fig. 1 of Le Petit et al. 2002). This can be summarized over a sightline by

$$f(HD) \leq f(H_2), \tag{2}$$

while the molecular fractions are linked together by

$$\left(\frac{D}{H}\right)_{ISM} = \frac{f(H_2)}{f(HD)} \times \frac{N(HD)}{2N(H_2)}. \tag{3}$$

The average value of $N(HD)/2N(H_2)$ noted above should therefore only be taken as a stringent lower limit to the $(D/H)_{ISM}$. Since the two molecular fractions reflect the average effectiveness of the self-shielding of each species, they should be highly correlated, even when summing over multiple clouds. Unlike the top panel, the bottom panel of Fig. 5 shows an increasing trend for $N(HD)/2N(H_2)$ as a function of $f(H_2)$ – and therefore a correlation between $f(HD)$ and $f(H_2)$ – consistent with predictions from models of the chemistry of HD (Le Petit et al. 2002).

Toward our highly reddened targets, atomic deuterium is blended by saturated hydrogen lines, and almost impossible to measure; direct comparison between the two molecular fractions is not feasible. We therefore used the two (D/H) ratios noted above (Jenkins et al. 1999; Moos et al. 2002) to examine $f(HD)$ vs. $f(H_2)$ (Fig. 6). The increasing trend is obvious. If the relation between $f(HD)$ and $f(H_2)$ can be understood, it could enable a wider survey of the D/H ratio via observations of HD. The apparent correlation between the molecular fractions should first be confirmed by observing targets in which both D and HD are measurable. That, however, requires targets with low overall column density but high $f(H_2)$. Another possibility would be to examine individual clouds, using very high resolution data in the FUV (unfortunately not available at present).

Further chemical modeling of diffuse clouds, including sums over a statistical distribution of diverse sizes and densities, could serve both to confirm the correlations and also to reveal other important parameters linked to the abundance of HD. For example, the formation rate of HD (and therefore the molecular fraction) is directly proportional to the ionization of H and H_2 by cosmic rays (Federman et al. 1996; Le Petit et al. 2002). It has been suggested that the observed abundances of H_3^+ in some diffuse lines of sight require a high flux of cosmic rays (Cecchi-Pestellini & Dalgarno 2000; McCall et al. 2003; Le Petit et al. 2004) and that the flux of cosmic rays could be very inhomogeneous in the diffuse ISM (for example due to variation in the magnetic field). The relationship between the molecular fractions of H_2 and HD would provide information on the formation rates of both molecules and on the flux of cosmic rays; the variations could give some indication of the level of inhomogeneities in the cosmic ray flux.

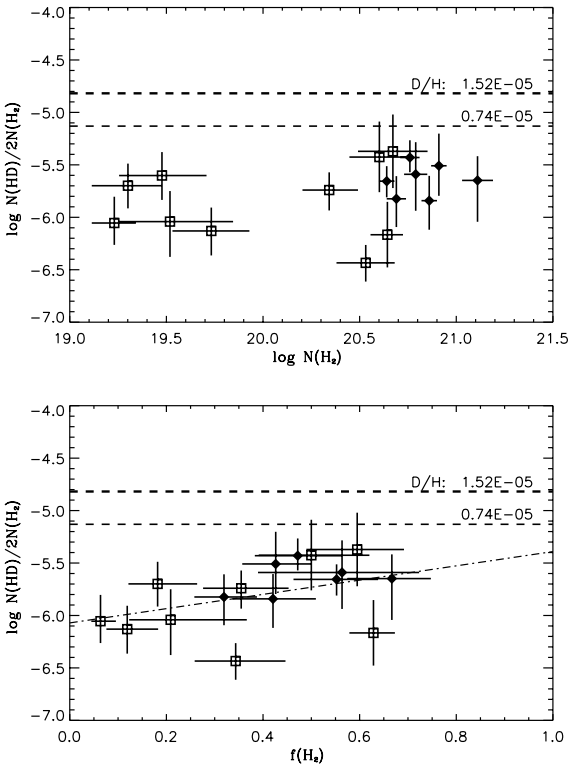

Fig. 5. N(HD)/2N(H_2) vs. N(H_2) and f(H_2). The upper dotted line gives the LISM D/H value (1.5×10^{-5}) found by Moos et al. (2002); the lower dotted line gives the D/H value found toward δ Ori (0.74×10^{-5}) by Jenkins et al. (1999), representative of the lower D/H values found in several other studies. Except for two sigthlines, we note an increasing trend with the molecular fraction which does not occur as a function of the molecular column density. It could be an indication that N(HD)/2N(H_2) did not reach the D/H value in the sightlines, showing therefore the importance of examining sightlines or clouds with higher f(H_2). Filled diamonds have N(HD) derived from *FUSE* spectra; open squares have N(HD) derived from reanalysis of *Copernicus* data.

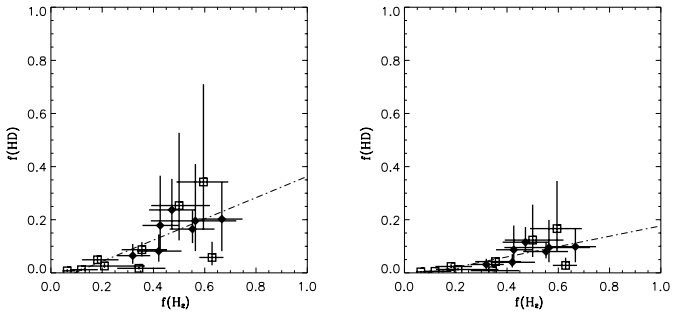

Fig. 6. f(HD) vs. f(H_2). The left panel assumes that $(D/H)_{ISM} = 0.74\times10^{-5}$, and the right panel assumes that $(D/H)_{ISM} = 1.52\times10^{-5}$. Both panels show a clear correlation between the molecular fractions. Understanding this correlation might provide a way to deduce $(D/H)_{ISM}$ from HD. Filled diamonds have N(HD) derived from *FUSE* spectra; open squares have N(HD) derived from reanalysis of *Copernicus* data (see Sect. 5.1).

5.3. Summary

We derived column densities of HD for 7 reddened sightlines using far-UV spectra obtained with the *FUSE* telescope. Most of the HD lines available in the far-UV are strongly affected by saturation (see the COG plotted in Fig. 2). We used high resolution optical CH data to determine the velocity structure in these sightlines, which allowed us to correct for the that saturation. The analysis was done using both curve of growth and profile fitting methods.

We combined our new results for HD with re-analyzed *Copernicus* measurements and compared the column densities of HD, H_2, and CH. A correlation between the HD and CH column densities is likely, but further measurements at low column densities are needed.

Simulations (Le Petit et al. 2002) have predicted for a one-cloud model with $A_V \sim 1$ mag a N(HD)/2N(H_2) ratio equal to the D/H ratio, and lower for thinner clouds. All our sightlines have $A_V > 1$, but are unfortunately composed of multiple clouds. We therefore obtained only stringent lower limits for $(D/H)_{ISM}$ ranging from 3.7×10^{-7} to 4.3×10^{-6}. We also noted a correlation between the molecular fraction of H_2 and the ratio N(HD)/2N(H_2) which we linked to a relationship between the self-shielding of H_2 and HD. If that relationship is confirmed, it would give a mean to infer $(D/H)_{ISM}$ from observations of HD.

Acknowledgements. This work is based on data obtained for the Guaranteed Time Team by the NASA-CNES-CSA *FUSE* mission operated by the Johns Hopkins University. This work has been done using the profile fitting procedure *Owens.f* developed by M. Lemoine and the *FUSE* French Team. This research has also made use of the FUSE database, operated at IAP, Paris, France. Financial support to U.S. participants has been provided by NASA contract NAS5-32985. Financial support to French Participants has been provided by CNES. D. E. Welty acknowledges support from the NASA LSTA grant NAG5-11413 to the University of Chicago.

References

Abgrall, H., Roueff, E., Launay, F., Roncin, J. Y., & Subtil, J. L. 1993a, A&AS, 101, 273
Abgrall, H., Roueff, E., Launay, F., Roncin, J. Y., & Subtil, J. L. 1993b, A&AS, 101, 323
Abgrall, H., Roueff, E., & Drira, I. 2000, A&AS, 141, 297
Allison, A. C., & Dalgarno, A. 1969, Atomic Data, 1, 289
André, M. K., Le Petit, F., Sonnentrucker, P., et al. 2004, A&A, 422, 483
Bertoldi, F., Timmermann, R., Rosenthal, D., Drapatz, S., & Wright, C. M. 1999, A&A, 346, 267
Black, J. H., & Dalgarno, A. 1973, ApJ, 184, L101
Bluhm, H., & de Boer, K. S. 2001, A&A, 379, 82
Catanzaro, G., André, M. K., Leone, F., & Sonnentrucker, P. 2003, A&A, 404, 677
Cecchi-Pestellini, C., & Dalgarno, A. 2000, MNRAS, 313, L6
Coc, A., Vangioni-Flam, E., Descouvemont, P., Adahchour, A., & Angulo, C. 2004, ApJ, 600, 544
Crawford, I. A. 1995, MNRAS, 277, 458
Dabrowski, I., & Herzberg, G. 1976, Can. J. Phys., 54, 525
Danks, A. C., Federman, S. R., & Lambert, D. L. 1984, A&A, 130, 62
de Zeeuw, P. T., Hoogerwerf, R., de Bruijne, J. H. J., Brown, A. G. A., & Blaauw, A. 1999, AJ, 117, 354
Federman, S. R., Strom, C. J., Lambert, D. L., et al. 1994, ApJ, 424, 772
Federman, S. R., Weber, J., & Lambert, D. L. 1996, ApJ, 463, 181

Ferlet, R., André, M., Hébrard, G., et al. 2000, ApJ, 538, L69
Fitzpatrick, E. L., & Massa, D. 1988, ApJ, 328, 734
Fitzpatrick, E. L., & Massa, D. 1990, ApJS, 72, 163
Hébrard, G., & Moos, H. W. 2003, ApJ, 599, 297
Hébrard, G., Lemoine, M., Vidal-Madjar, A., et al. 2002, ApJS, 140, 103
Hoopes, C. G., Sembach, K. R., Hébrard, G., Moos, H. W., & Knauth, D. C. 2003, ApJ, 586, 1094
Horne, K. 1986, PASP, 98, 609
Humphreys, R. M. 1978, ApJS, 38, 309
Jenkins, E. B., Tripp, T. M., Woźniak, P., Sofia, U. J., & Sonneborn, G. 1999, ApJ, 520, 182
Laurent, C., Vidal-Madjar, A., & York, D. G. 1979, ApJ, 229, 923
Le Petit, F., Roueff, E., & Herbst, E. 2004, A&A, 417, 993
Le Petit, F., Roueff, E., & Le Bourlot, J. 2002, A&A, 390, 369
Lemoine, M., Audouze, J., Ben Jaffel, L., et al. 1999, New Astron., 4, 231
Lemoine, M., Vidal-Madjar, A., Hébrard, G., et al. 2002, ApJS, 140, 67
Lynds, B. T. 1962, ApJS, 7, 1
Magnani, L., Onello, J. S., Adams, N. G., Hartmann, D., & Thaddeus, P. 1998, ApJ, 504, 290
McCall, B. J., Huneycutt, A. J., Saykally, R. J., et al. 2003, Nature, 422, 500
Moos, H. W., Cash, W. C., Cowie, L. L., et al. 2000, ApJ, 538, L1
Moos, H. W., Sembach, K. R., Vidal-Madjar, A., et al. 2002, ApJS, 140, 3
Morbidelli, L., Patriarchi, P., Perinotto, M., Barbaro, G., & di Bartolomeo, A. 1997, A&A, 327, 125
Pan, K., Federman, S. R., & Welty, D. E. 2001, ApJ, 558, L105
Rachford, B. L., Snow, T. P., Tumlinson, J., et al. 2001, ApJ, 555, 839
Rachford, B. L., Snow, T. P., Tumlinson, J., et al. 2002, ApJ, 577, 221
Robertson, J. G. 1986, PASP, 98, 1220
Rogerson, J. B., & Ewell, M. W. 1985, ApJS, 58, 265
Rogerson, J. B., & Upson, W. L. 1977, ApJS, 35, 37
Sahnow, D. J., Moos, H. W., Ake, T. B., et al. 2000, ApJ, 538, L7
Sembach, K. R., & Savage, B. D. 1992, ApJS, 83, 147
Snow, T. P. 1975, ApJ, 201, L21
Snow, T. P. 1976, ApJ, 204, 759
Snow, T. P. 1977, ApJ, 216, 724
Snow, T. P., Rachford, B. L., Tumlinson, J., et al. 2000, ApJ, 538, L65
Sonneborn, G., Tripp, T. M., Ferlet, R., et al. 2000, ApJ, 545, 277
Sonnentrucker, P., Friedman, S. D., Welty, D. E., York, D. G., & Snow, T. P. 2002, ApJ, 576, 241
Sonnentrucker, P., Friedman, S. D., Welty, D. E., York, D. G., & Snow, T. P. 2003, ApJ, 596, 350
Spitzer, L., Drake, J. F., Jenkins, E. B., et al. 1973, ApJ, 181, L116
St.-Louis, N., & Smith, L. J. 1991, A&A, 252, 781
Thorburn, J. A., Hobbs, L. M., McCall, B. J., et al. 2003, ApJ, 584, 339
van Dishoeck, E. F., & Black, J. H. 1989, ApJ, 340, 273
Vangioni-Flam, E., Coc, A., & Cassé, M. 2000, A&A, 360, 15
Watson, W. D. 1973, ApJ, 182, L73
Welty, D. E., & Hobbs, L. M. 2001, ApJS, 133, 345
Wood, B. E., Linsky, J. L., Hébrard, G., et al. 2004, ApJ, 609, 838
Wright, C. M., van Dishoeck, E. F., Cox, P., Sidher, S. D., & Kessler, M. F. 1999, ApJ, 515, L29
Wright, E. L., & Morton, D. C. 1979, ApJ, 227, 483